Fusion of airborne LiDAR and multispectral sensors reveals synergic capabilities in forest structure characterization

Jose A. Manzanera, Antonio García-Abril, Cristina Pascual, Rosario Tejera, Susana Martín-Fernández, Timo Tokola & Ruben Valbuena

Taylor & Francis
Taylor & Francis Group

Fusion of airborne LiDAR and multispectral sensors reveals synergic capabilities in forest structure characterization

Jose A. Manzanera[a]*, Antonio García-Abril[a], Cristina Pascual[a], Rosario Tejera[a], Susana Martín-Fernández[a], Timo Tokola[b] and Ruben Valbuena [b]

[a]College of Forestry and Natural Environment, Research Group SILVANET, Universidad Politecnica de Madrid, Ciudad Universitaria, 28040, Madrid, Spain; [b]Faculty of Science and Forestry, University of Eastern Finland, Joensuu, Finland

Forest stand structure is an important concept for ecology and planning in sustainable forest management. In this article, we consider that the incorporation of complementary multispectral information from optical sensors to Light Detection and Ranging (LiDAR) may be advantageous, especially through data fusion by back-projecting the LiDAR points onto the multispectral image. A multivariate data set of both LiDAR and multispectral metrics was related with a multivariate data set of stand structural variables measured in a Scots pine forest through canonical correlation analysis (CCA). Four statistically significant pairs of canonical variables were found, which explained 83.0% accumulated variance. The first pair of canonical variables related indicators of stand development, i.e. height and volume, with LiDAR height metrics. CCA also found attributes describing stand density to be related to LiDAR and spectral variables determining canopy coverage. Other canonical variables pertained to Lorenz curve-derived attributes, which are measures of within-stand tree size variability and heterogeneity, able to discriminate even-sized from uneven-sized stands. The most relevant result was to find that metrics derived from the multispectral sensor showed significant explanatory potential for the prediction of these structural attributes. Therefore, we concluded that metrics derived from the optical sensor have potential for complementing the information from the LiDAR sensor in describing structural properties of forest stands. We recommend the use of backprojecting for jointly exploiting the synergies of both sensors using similar types of metrics as they are customary in forestry applications of LiDAR.

Keywords: airborne laser scanning; data fusion; forest Structural Types; multispectral imagery; Stand structure

Introduction

Forest multifunctionality is an intrinsic manifold value based on stand structure (McElhinny et al. 2005). Variability in tree sizes is intimately related to canopy structure (Valbuena et al. 2012a) and light penetration (Montgomery and Chazdon 2001; Saremi et al. 2014) and hence to biodiversity (McArthur and McArthur 1961). Forest management may alter tree size distribution and natural dynamics, with implications for the conservation of natural resources (Lähde et al. 1991; Maltamo, Uuttera, and Kuusela 1997; Valbuena et al. 2016). In order to quantitatively assess forest structure, several

---

*Corresponding author. Email: joseantonio.manzanera@upm.es

indices have been developed to describe the structural complexity of forest stands (Lexerød and Eid 2006; von Gadow et al. 2012; Valbuena 2015). Structure indices can improve predictions of forest dynamics models (Lei, Wang, and Peng 2009), help in assessing the protective function of forest ecosystems (Bachofen and Zingg 2001), and in planning sustainable management (Buongiorno et al. 1994). Such structure indices are often prohibitive to implement at landscape or regional scales as they require extensive inventories to achieve sufficient statistical precision by ordinary sampling methods. However, with the advent of LiDAR (Light Detection and Ranging), these structure indices may be more readily calibrated and spatially quantified. LiDAR has been recognized as an outstanding active remote sensing tool for making measurements of tree height (Andersen, Reutebuch, and McGaughey 2006; Estornell et al. 2014), canopy size, and modeling (Van Leeuwen, Coops, and Wulder 2010), forest inventory (Naesset 2002; Chen and Zhu 2013), forest fuel modeling (Arroyo, Pascual, and Manzanera 2008; Garcia et al. 2011), forest structure characterization (Pascual et al. 2008), etc. The vertical distribution of a vegetation canopy can be assessed from the characteristics of the LiDAR waveform (or the distribution of discrete returns) to predict attributes related to stand structure. Using canonical correlation analysis (CCA), Lefsky et al. (2005a) defined pairs of canonical correlation components which represented axes of variation in the canopy and stand structure data sets, coherently linked to associated patterns of variation in statistical metrics derived from the LiDAR return distribution.

Those initial studies of forest structure, inferred from LiDAR, were further advanced by incorporating predictors derived from satellite multispectral data sets (Pascual et al. 2010). Data fusion of both LiDAR and optical passive sensors, such as multispectral photography, have synergistic capabilities for providing reliable inventories for operational forestry (Packalén, Suvanto, and Maltamo 2009; Valbuena et al. 2013). Estimation of forest parameters from LiDAR can also be enhanced by image analysis, exploiting the potential of spectral imagery for thematic classification and index calculation (St-Onge and Achaichia 2001; Zhang, Xie, and Selch 2013; Chu et al. 2016), along with the accuracy of tree height information retrieved from LiDAR (Lefsky et al. 1999). Even species-specific estimations can be obtained by combining variables derived from both LiDAR and multispectral sensors (Koukoulas and Blackburn 2005; Packalén and Maltamo 2006).

Despite these successes, the correct spatial adjustment of the information derived from diverse sensors is an important challenge (Honkavaara et al. 2006). Geometrical errors affect radiometric quality in that they lead to locating a different digital number (DN) than the one actually corresponding to a determined geographical position. Practitioners often encounter problems of data mismatching (e.g. Valbuena et al. 2011; Bright, Hicke, and Hudak 2012). Therefore, the precision offered by remote sensors has to be accompanied by accurate georeferencing (Hyyppä et al. 2000; Valbuena 2014). The most common data fusion approach used is, in the case of digital camera images, orthorectification and fusion of rasterized data at the pixel level (Pohl and Van Genderen 1998). However, lack of correspondence between the LiDAR and multispectral data sets may severely affect their simultaneous application in practice (Bright, Hicke, and Hudak 2012). This contingency is sometimes overcome by manual editing or including additional control points from the LiDAR data set itself (Garcia et al. 2011). Appropriate automated geometric correspondence of simultaneously acquired LiDAR and aerial multispectral imagery, plus the positioning of LiDAR points on the perspective projection of uncorrected aerial pictures resulted in the successful allocation of the original radiometric information in the LiDAR point cloud (Valbuena et al. 2011). This

method, known as back-projecting (Figure 1), is becoming widespread in fine-scale studies which exploit the full potential of both sensors (Packalén, Suvanto, and Maltamo 2009; Ørka et al. 2012; Valbuena et al. 2013).

The objectives of this research are based on the foundations from Lefsky et al. (2005b), and the new possibilities of this burgeoning back-projecting method. They observed patterns of covariance between LiDAR metrics and forest variables describing (in order of amount of explained variability): stand height, density, and heterogeneity. Pascual et al. (2010) added metrics derived from satellite coarse imagery, finding synergies with the LiDAR metrics. To date, errors in data correspondence may have impeded a comprehensive study of these relations with very high-resolution multispectral imagery (Bright, Hicke, and Hudak 2012). The virtually perfect matching that is achieved by back-projection (Valbuena 2014) permits a deeper analysis on patterns of covariance to forest structure properties (Lefsky et al. 2005b), using both sensors simultaneously. The goal of this study is therefore to analyze the canonical relationship between two coincident multivariate data sets, one containing both LiDAR and passive optical sensor measurements, and the other containing field measurements of stand structure. This will lead to benefit from the optical sensor potential for complementing the information from the LiDAR sensor in describing structural properties of forest stands, and from the information availability of within-stand tree size variability and heterogeneity, for environmental management purposes.

Material and methods

Study area and field measurements

The study area was located in Valsaín (Spain; latitude: 40°53′–41°15′N; longitude: 3°59′–4°18′W; altitude 1300–1500 m above sea level), a forest attached to the Sierra de Guadarrama National Park with Scots pine (*Pinus sylvestris* L.) as the main species. The field survey consisted of 37 circular plots of 20 m radius sampled in a cluster design (e.g. Chuvieco 2007), where diameter at breast height (*dbh*, cm) and tree top height (*h*, m) were recorded for every tree within the plot for *dbh* classes >10 cm. Diameters were measured with a caliper in two perpendicular directions which were later averaged, and heights were determined with a Vertex III Hypsometer (Haglof, Sweden). Saplings with *dbh* <10 cm were measured only within 10 m from plot center, and they were repeated fourfold after assuring within-plot homogeneity in the field.

Global Navigation Satellite Systems (GNSS) static observations were recorded at each plot center with a survey-grade HiPer-Pro receiver (Topcon, California) for at least 30 min, during the time spent for forest mensuration. Consequently, GNSS acquisition time was not a limiting factor and GNSS accuracy was uninfluenced by the heterogeneity of structural types (Valbuena et al. 2012b). We acquired dual static observations at 1 Hz logging rates from both GPS and GLONASS (Global Navigation Satellite System) constellations. To diminish the multipath effect of the forested environment, we set the antenna at 1–2 m height and the mask at a cut-off angle of 15°. Differential corrections were computed according to the procedure described in Valbuena et al. (2012b). This surveying configuration was selected as previous research found it to be the most cost-efficient alternative providing centimeter accuracy (Valbuena et al. 2010), and therefore GNSS positional errors (twice the distance root mean square [2dRMS] = 1.34 m; circular error 50% probability [CEP50] = 0.56 m; and spherical error 50% probability [SEP50] = 0.59 m) were assured not to negatively affect forest response computation (Mauro et al. 2011).
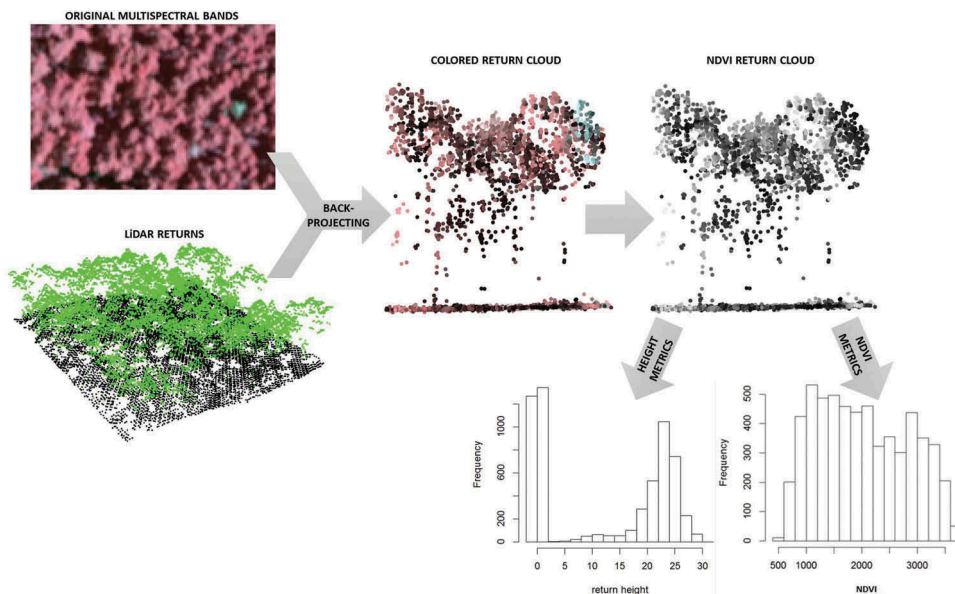
Figure 1.   Schematic representation of the method of back-projecting the spectral information (photography) into the LiDAR data set. The spectral information (upper left photo) is geometrically integrated with the LiDAR data (lower left; see details in the text). The resulting data set renders a colored point cloud from which metrics from both LiDAR (e.g. height, m) and Normalized Difference Vegetation Index (*NDVI*, in digital numbers) have been extracted and analyzed. For full color versions of the figures in this paper, please see the online version.

Forest structural attributes

Forest stand structural attributes were computed from these field data at the plot-level: stem density (N, stems ha^{-1}), quadratic mean diameter (D_g, cm), Lorey's height (H_L, m), standing volume (V, m^3 ha^{-1}), Stand Density Index (*SDI*), Gini coefficient (*GC*), Lorenz asymmetry (L_a), and the proportions of basal area and number of stems larger than the D_g (*BALM* and *NSLM*, respectively). The most common variables of wood stocking used in forest management are N and the basal area, the cross-sectional area at breast height occupied by trees. Therefore, the most adequate descriptors of average *h* and *dbh* at plot and stand-level typically are basal area-weighted (Curtis and Marshall 2000). Thus, we computed H_L and D_g, variables which have been successfully predicted from ALS (airborne laser scanning) remote sensing (Naesset 2002). Calculations of *V* were aggregated from individual stem volume estimations using *dbh* and *h* in equations, with locally adjusted coefficients for *P. sylvestris* (Rojo and Montero 1996). The *SDI* was calculated according to Reineke (1933), so that it expressed the number of trees per hectare larger than a base diameter of 25.5 cm. Moreover, indicators of forest structure derived from Lorenz curves were also calculated at the plot level (Valbuena et al. 2014). The *GC* is a simple indicator of inequality of sizes among the trees (Valbuena et al. 2016), because it has been suggested as a measured tree size heterogeneity dispersion that is superior to variance (Knox, Peet, and Christensen 1989) or structural diversity indices (Valbuena et al. 2012a). We calculated *GC* as the average of basal area-weighted tree-by-tree differences for all trees within a sample plot. L_a measures the asymmetry of the Lorenz curve (Damgaard and Weiner 2000), and it can be disaggregated into its separate components:

NSLM and *BALM* (Gove 2004). L_a, *BALM,* and *NSLM* can be used to evaluate relations of relative dominance between overstory and understory (Valbuena 2015).

Sensors

Remote sensing data were simultaneously acquired with a discrete-pulse multi-return airborne laser scanner (ALS50-II) (Leica Geosystems, Switzerland), and a digital mapping camera (Zeiss-Intergraph, Germany) system consisting of four charge-coupled device (CCD) frame array sensors. Both sensors were mounted on board a 404-Titan (Cessna, Kansas) with a double photogrammetric window, which flew in clear sky conditions at about 1500 m above terrain level with a ground speed of 72 m s^{-1}. On-flight GNSS and inertial navigation systems (INS) provided the position and attitude of each sensor. Planimetric coordinates were represented in the European Terrestrial Reference System 1989 (ETRS89), using the Universal Transverse Mercator projection, zone 30°N. Orthometric altitudes were obtained according to the Ibergeo95 geoid model (Sevilla 1995), and the altimetric datum was the mean sea level in Alicante, Spain.

LiDAR

The flight covered four ALS scan lines of 665 m swath width with a 40% side lap. An intensity value was recorded by the ALS50-II sensor for each one of a maximum of four discrete returns per pulse. Pulse frequency was set to 55 kHz, footprint diameter was about 0.5 m at nadir and the average pulse density was 1.15 pulses m^{-2}. For the given surveying conditions, the precision of both vertical and horizontal coordinates for returns is 0.17 m (Baltsavias 1999). Elevation differences between overlapping strips were under sensor tolerance, so that the resulting returns in laser (LAS) file format (version 1.3, American Society for Photogrammetry and Remote Sensing (ASPRS) Standards Committee 2010) were georeferenced without additional adjustments. Ground returns were filtered following Axelsson (2000), by iteratively including into a triangulated irregular network (TIN), the lowest elevation returns within 2 m below a threshold angle ranging between 12° and 75°. Points included in the TIN were classified as ground, and the remaining as vegetation. Terrain was characterized by a Digital Terrain Model (DTM) of 1 m pixel size interpolated from ground points. The quality control by ground surveying provided a precision of 15 cm. The heights of all ALS returns above ground level were obtained by subtracting the DTM value at their horizontal coordinates. Height metrics (denoted as *Height*.) were generated from the point cloud with the command *cloudmetrics* of FUSION software for data analysis (McGaughey 2012), following the technique described in Valbuena et al. (2013).

Multispectral imagery and back-projection

Optical sensor images were captured at a 5-ms exposure time with a 60% forward overlap and 40% side lap. For the purpose of this work, we used only the scenes obtained from the multispectral heads with selective sensitivity for red (*Red*, 580–690 nm) and near-infrared (*NIR*, 700–1050 nm). The original 12 bit radiometric resolution was linearly stretched to increase their dynamic range to 16 bit (2 byte) DNs in tagged image file format (version 6.0, Adobe Systems, 1992). Spatial resolution was 60 cm, as *Red* and *NIR* heads had a focal length of 30 mm (Photo scale reciprocal: 50,000) and

CCD capacitors sized 12 μm. Original distortion-free and principal point corrected (Dörstel, Jacobsen, and Stallmann 2003) imagery was used with no further orthorectification procedure. Direct GNSS/INS georeferencing and ground control point aerotriangulation were combined to obtain the final external orientation parameters for each image. With *Red* and *NIR* data we generated the Normalized Difference Vegetation Index (*NDVI*; Rouse et al. 1974):

$$\text{NDVI} = \frac{(\text{NIR} - \text{Red})}{(\text{NIR} + \text{Red})} \tag{1}$$

Data fusion was carried out by means of the back-projecting method (Valbuena 2014), which secures proper correspondence between the sensors, compared to the most customary approach of orthorectifying the multispectral imagery (Valbuena et al. 2011). Back-projecting consists in rendering LiDAR from the optical camera's perspective to extract the camera information that corresponds to each return. That information is then fetched and retrieved back to the original position of the LiDAR returns, effectively coloring them (Figure 1) while avoiding extra requirements needed for orthorectification which are error prone: an assumption of the height (usually taken from the DTM), bundle adjustment, seamless mosaicking techniques, etc. The back-projection is carried out applying information about the optical sensor architecture (internal orientation) and the platform position and bearing (external orientation) into the collinearity principle. In the case of this study, the information retrieved was not the DNs from the original bands, but the values of *NDVI* instead, which were stored in a channel field in the LAS files (ASPRS Standards Committee 2010). This way, it was possible to compute metrics (denoted as *ndvi.*) describing the distribution of *NDVI* values directly from the point cloud using FUSION software, in a similar manner as it is customarily done for the height metrics from LiDAR (Figure 1; McGaughey 2012).

Exploratory multivariate analysis

CCA was performed to assess the interrelationships between two data sets of variables: LiDAR and multispectral metrics, on one side (the predictor data set), and forest structure indicators derived from field measurements averaged at the plot level, from the other (the response data set). In each of the predictor and response data sets, correlation matrices were calculated. When a pair of variables had an absolute value of the correlation coefficient of 0.87 or higher, one of them was excluded from the CCA. The CCA was iteratively performed by eliminating supererogatory variables which surpassed the 0.87 absolute value of the correlation-level with other variables of the same set, until the correlation matrix of the remaining variables could be inverted and the regression equation could be evaluated. The Canonical Analysis package of Statistica (version 7.1, StatSoft Inc., Tulsa, OK) was used. The amount of explained variance was calculated using the canonical *R*-square, and the significance of CCA components was evaluated using χ^2 and Wilk's lambda tests. The importance of each variable in both the predictor and response data set was assessed evaluating its correlation to each of the significant CCA components.

Results

From the initial set of variables describing forest structure indicators (N, D_g, H_L, V, SDI, GC, L_a, $BALM$ and $NSLM$), two of them were excluded because they showed an absolute value of the correlation coefficient higher than 0.87 with other variables of stand structure. D_g showed high linear correlation with SDI ($r = 0.997$, $p < 0.001$) and with N ($r = 0.914$, $p < 0.001$). Also, the correlation matrix could not be inverted when $NSLM$ was selected, so we opted to reduce the multivariable set to six variables, by retaining SDI, which is a function of both N and D_g, and excluding N, D_g, and $NSLM$ out from further analysis.

For similar reasons, out of the 90 LiDAR and optical metrics provided by FUSION, we chose 20 variables showing an absolute value of the correlation coefficient lower than 0.87 to one another. Among the FUSION-generated LiDAR metrics, we selected: the height maximum (*Height.Max*), mean (*Height.Mean*), minimum (*Height.Min*), mode (*Height.Mode*), the height percentiles 5th (*Height.P05*), 30th (*Height.P30*), and 40th (*Height.P40*), the median of the absolute deviations from the overall median (*Height. MADmedian*), the canopy relief ratio (*Height.CRR*), the number (*Height.F1 m*) and proportion (*Height.PropF1 m*) of first returns above 1 m height, the number of modes (*Height.KDEmodes*), and the minimum mode (*Height.KDEminMode*) in the kernel-estimated probability density function of the point heights in the sample. Regarding the metrics derived from the *NDVI* (Equation 1) values obtained in those same back-projected LiDAR returns, we chose the following variables under similar criteria: maximum of *NDVI* (*ndvi.Max*), mean (*ndvi.Mean*), minimum (*ndvi.Min*), mode (*ndvi.Mode*), inter quartile range (*ndvi.IQR*), *L*-kurtosis coefficient (*ndvi.Lkurt*), and the *NDVI* 95th (*ndvi.P95*) percentile. It is worth noting that we observed in general low-to-moderate correlations ($|r| < 0.64$) between LiDAR height and *NDVI* variables.

The overall canonical coefficient of correlation ($R = 0.995$) was highly significant ($p = 0.000$). The total redundancy indicated that, on the average, 84.92% of the variance in the set of stand structure variables could be explained by the set of LiDAR plus spectral metrics. Likewise, a 60.63% variance of the second set could be accounted for, given the first (Table 1). The four first pairs of canonical variables were statistically significant at the 95% level of confidence ($p < 0.05$; Table 1). The correlation coefficients between the significant pairs of canonical variables for the two data sets

Table 1. Summary of canonical correlation analysis, with a set of six variables of forest structure (Variance extracted: 100.00%; Total redundancy: 84.92%) and a set of 20 variables of LiDAR and *NDVI* metrics (Variance extracted: 60.63%; Total redundancy: 53.69%).

Root removed	Canonical R	Canonical R^2	χ^2	df	p	Wilk's Lambda
		Chi-square tests with successive roots removed				
0	0.9949	0.9899	286.8934	120	0.0000	0.0000
1	0.9811	0.9626	183.5842	95	0.0000	0.0003
2	0.9083	0.8250	109.6567	72	0.0029	0.0076
3	0.8833	0.7801	70.4407	51	0.0371	0.0437
4	0.7990	0.6383	36.3581	32	0.2729	0.1987
5	0.6712	0.4506	13.4746	15	0.5657	0.5494

df: Degrees of freedom; LiDAR: Light Detection and Ranging; *NDVI*: Normalized Difference Vegetation Index.

Table 2.   Correlations between forest structure indices and their canonical variables.

Response variable	CCA1	CCA2	CCA3	CCA4
SDI	0.746	−0.137	**−0.634**	0.117
p value	0.000	0.420	0.000	0.492
HL	**0.965**	−0.186	0.150	−0.069
p value	0.000	0.271	0.374	0.684
V	**0.900**	**0.346**	0.083	−0.233
p value	0.000	0.036	0.626	0.166
GC	−0.579	−0.264	**0.616**	**−0.318**
p value	0.000	0.114	0.000	0.055
L_a	0.243	−0.184	−0.503	−0.262
p value	0.148	0.277	0.002	0.117
BALM	−0.356	**−0.372**	0.370	**−0.549**
p value	0.031	0.023	0.024	0.000
VE	0.470	0.069	0.200	0.091
Accumulated VE	0.470	0.539	0.739	0.830
Redundancy	0.465	0.067	0.165	0.071
Accumulated redundancy	0.465	0.531	0.697	0.767

The numbers in bold (absolute values) indicate the top 33th percentile of correlations of forest structure indices with each canonical variable. VE, accumulated VE, redundancy, and accumulated redundancy for the four response canonical components are shown. VE: Variance extracted.

(predictors vs. response) ranged from 0.883 to 0.995. The amount of variance explained in the response component ranged between 78.01% and 98.99%, as observed in the R^2 obtained. The Wilk's Lambda test for hypothesis that all these four canonical variables were equal to zero was rejected ($p < 0.05$; Table 1). The correlations between forest structure variables and their canonical variables (Table 2) revealed that, in total, 83.0% accumulated variance was explained by the four significant canonical components. This variance was explained using 48.6% of the total variance in the predictor data set (Table 3).

Discussion

The back-projecting technique, from which the original spectral information of aerial images and the deriving vegetation indices are attached to each LiDAR discrete return, has proven to be an accurate method for fusing these data sets, particularly when both are large (Torabzadeh, Morsdorf, and Schaepman 2014). This technique adds the advantage of keeping the radiometric integrity by simplifying procedures and avoiding both height gridding and radiometry resampling. Its superiority to the traditional fusion of orthophotos with LiDAR data in grid format (Torabzadeh, Morsdorf, and Schaepman 2014) was demonstrated previously (Valbuena et al. 2011). A 0.11-m horizontal error and a 0.21-m RMSE were obtained for the back-projecting-generated imagery in a forest area, while the horizontal error raised to 1.77–2.08 m and the RMSE to 2.15–2.79 m, when traditional or true-orthorectification images were used at a 15-cm spatial resolution (Valbuena et al. 2011). Wu et al. (2015) also found similar results after the integration of LiDAR data with satellite imagery in an urban area, where the horizontal error was 0.65 m, while without data fusion the error raised to 1.87 m. These results support our choice for back-projecting as the best available method for LiDAR and spectral imagery data fusion.

Table 3. Correlations between LiDAR predictors – height and *NDVI* metrics – and their canonical variables.

Predictor variable	CCA1	CCA2	CCA3	CCA4
Height.Max	**0.767**	−0.210	**0.327**	0.179
p value	0.000	0.213	0.048	0.290
Height.Mean	**0.937**	0.193	0.139	−0.145
p value	0.000	0.252	0.411	0.392
Height.min	−0.118	0.000	−0.019	−0.052
p value	0.485	1.000	0.912	0.762
Height.mode	−0.577	−0.231	−0.180	0.053
p value	0.000	0.168	0.286	0.754
Height.P05	0.593	0.148	**0.477**	−0.153
p value	0.000	0.383	0.003	0.365
Height.P30	−0.084	0.230	**0.318**	−0.089
p value	0.620	0.171	0.055	0.601
Height.P40	0.520	**0.734**	0.147	−0.148
p value	0.001	0.000	0.387	0.384
Height.MAD.median	−0.403	**−0.627**	−0.089	0.030
p value	0.013	0.000	0.602	0.861
Height.CRR	**0.732**	0.430	−0.015	**−0.292**
p value	0.000	0.008	0.929	0.080
Height.F1 m	**0.748**	0.262	0.188	0.019
p value	0.000	0.117	0.266	0.911
Height.PropF1 m	−0.193	**0.703**	**0.564**	−0.056
p value	0.253	0.000	0.000	0.740
Height.KDEmodes	−0.287	0.075	0.201	**0.333**
p value	0.085	0.661	0.233	0.044
Height.KDEminMode	**−0.626**	−0.140	**0.512**	0.100
p value	0.000	0.410	0.001	0.558
ndvi.Max	−0.022	0.200	0.170	0.078
p value	0.898	0.235	0.314	0.648
ndvi.Mean	0.232	**0.593**	0.282	**0.208**
p value	0.167	0.000	0.091	0.216
ndvi.Min	−0.165	0.355	0.317	**0.269**
p value	0.329	0.031	0.056	0.107
ndvi.Mode	0.081	0.321	0.201	0.050
p value	0.636	0.053	0.233	0.770
ndvi.IQR	−0.410	**−0.662**	−0.208	−0.181
p value	0.012	0.000	0.217	0.283
ndvi.L kurt	0.547	0.253	−0.193	**−0.277**
p value	0.001	0.131	0.253	0.098
ndvi.P95	0.004	0.376	0.190	0.145
p value	0.979	0.022	0.260	0.394
VE	0.213	0.188	0.058	0.027
Accumulated VE	0.213	0.401	0.459	0.486
Redundancy	0.212	0.180	0.049	0.021
Accumulated redundancy	0.212	0.392	0.441	0.462

The numbers in bold (absolute values) indicate the top 25th percentile of correlations of forest structure indices with each canonical variable. VE, accumulated VE, redundancy, and accumulated redundancy for the four response canonical components are shown. VE: Variance extracted; LiDAR: Light Detection and Ranging; *NDVI*: Normalized Difference Vegetation Index.

Univariate ordinary least square regression relates a single dependent variable with multiple independent variables, while CCA relates multiple dependent variables with multiple independent variables. CCA has not been so popularly used in remote sensing

as univariate multiple regression methods. However, the advantages of CCA for remote sensing applications have been demonstrated and detailed (Cohen et al. 2003). The analysis of stand structure through CCA has provided a new understanding of the relationships between field measured Scots pine stand structural variables, on one side, and remotely sensed variables from LiDAR and multispectral sensors, on the other side. The four significant canonical pairs of variables obtained in the CCA analysis revealed the usefulness of the information provided by both LiDAR and multispectral sensors. The first pair of canonical variables highlighted the distinct performance of LiDAR height metrics (Table 3) in explaining tree height and standing volume (Table 2), as the main features representing the general development of the stand. Furthermore, the first pair of canonical variables explained the greatest part of the variability. The remaining pairs of canonical variables were related to variables describing stand density and structural heterogeneity. These results agree in general terms with those found by Lefsky et al. (2005b), who also explained stand height, aboveground biomass, cover, maturity, stand density, and other structural variables of ecological significance by CCA. Similarly, Sherrill, Lefsky, and Bradford (2008) found that the primary source of variability in canopy structure is related to height and biomass, and the second source of variability is related to tree density. Our results also indicate that the LiDAR sensor provided most of the significant metrics in this study (Table 3). Nevertheless, the multispectral sensor provided *NDVI* metrics, which explained heterogeneity, vigor, and maturity in the second and fourth pairs of canonical variables. This result has not been found previously and deserves further analysis. We interpret the relationships of LIDAR height and multispectral *NDVI* metrics to forest characteristics as shown in the four canonical variable pairs in detail in the next paragraphs.

Metrics relating to stand development

Correlations between stand structure indices and the canonical variables identified H_L ($r = 0.965$; $p = 0.000$) and V ($r = 0.900$; $p = 0.000$) as the most closely related indices to the first canonical component CCA1 (Table 2). On the other hand, the first canonical component in the response was highly correlated with height LiDAR metrics ($|r| = 0.626$–0.937), including the mean, the maximum, the number of first returns above 1 m height, the canopy relief ratio, which is the rank of heights normalized by their mean, and *Height.KDEminMode* (Table 3). This last variable, the minimum mode in the kernel-estimated probability density function for the point heights in the sample, showed an inverse relation with negative correlation with the first canonical component. This first canonical variable pair represents the general development of the stand, and accounts for the major part of the explained variability (47.0%). The predictors most relevant to this component CCA1 were mainly descriptors of the location and dispersion of LiDAR heights. Response variables were related to height and basal area, since H_L is basal area-weighted and V was calculated using both *dbh* and *h*. All the relevant relations in Tables 2–3 had positive signs except for *Height.KDEminMode*, and therefore the meaning of the first pair of canonical components is that the higher and more disperse the LiDAR returns are, the larger the height, diameters, and volume (and hence biomass) in the trees contained. These results are convergent with those presented by Lefsky et al. (2005b) and Sherrill, Lefsky, and Bradford (2008), who also reported high correlations of the first canonical variable with stand height variables. Our results agree, as the same

variable showed the highest correlation coefficient ($r = 0.965$), and standing volume, which is known to increase with stand height in many forests, was also highly correlated with CCA1.

Compared to the metrics computed from the LiDAR heights, those derived from the multispectral imagery had very little predictive power. Previous studies (Pascual et al. 2010) tried to relate LiDAR height metrics with multispectral indices derived from Landsat ETM+, such as Tasseled Cap and normalized difference indices, through Reduced Major Axis regression analysis. However, the spatial resolution of Landsat imagery and co-registration with LiDAR data limited the accuracy of characterizing forest structure (Pascual et al. 2010). Nevertheless, Packalén, Suvanto, and Maltamo (2009) and Ørka et al. (2012) stressed the potential of integrating both LiDAR and spectral sensors for increasing remote sensing's capacity for species identification. Further research should be conducted in mixed forests for this purpose.

Metrics relating to stand density

The second and third canonical variables were related to the percentage of first returns above 1 m, which is a proxy for vegetation cover (Andersen, Reutebuch, and McGaughey 2006; McGaughey 2012), and CCA2 was also related to the 40th percentile of canopy height. These indices represent medium height vegetation, meaning that these canonical pairs may be interpreted as being related to stand density. This was confirmed by the association of the third canonical component with the *SDI* (Table 2). The canonical variable CCA2 was also negatively correlated with the median of the absolute deviations from the overall median (*Height.MAD.median*), an indicator of open covers (Table 3). The positive association of CCA2 with the mean *NDVI* and the negative association with the *NDVI* interquartile range also indicate healthy, dense young vegetation (Table 3).

In the stand structure data set, the second canonical variable was positively related to the volume ($r = 0.346$, $p = 0.036$) and negatively to *BALM* ($r = -0.372$; $p = 0.023$; Table 2), the latter representing the proportion of basal area stocked above the quadratic mean diameter, and consequently, the balance among subpopulations within the stand (Gove 2004; Valbuena et al. 2014). Therefore, CCA2 is associated with the presence of young stems and CCA3 with *SDI*, overall indicating stand density, in conjunction with Lefsky et al. (2005b).

Metrics relating to tree size inequality

The *GC*, an indicator of tree size inequality (Valbuena et al. 2012a) was represented at the third and fourth canonical variables. The latter was associated to *Height.KDEmodes* (Table 3), which represents the number of mode values in the kernel density estimated probability function for the point heights in the sample, and it is therefore a surrogate for the number of tree layers in that forest. This variable is related to the presence of uneven sized vegetation or with gaps in between trees. Also, CCA3 was associated with both the 5th and 30th percentiles of height, which represent low and medium height vegetation, and it was also associated with the proportion of first returns above 1 m and with the maximum height (Table 3). These two last variables represent high vegetation. Therefore, the simultaneous combination of all these variable correlations is related to uneven-sized stands.

In the stand structure variables, the Lorenz curve-based index *GC* correlated ($r = 0.616$; $p = 0.000$; Table 2) with the corresponding stand structure canonical variable CCA3. As

higher values of *GC* denote size inequality, this relationship indicates the presence of an uneven-sized structure. The *GC* is an indicator of tree size inequality, i.e., valuable for discriminating even-sized from uneven-sized stands. Also, *SDI* was negatively correlated with CCA3 (Table 3). Thus, the third pair of canonical variables CCA3 was associated with the tree size distribution in the stand, discriminating even-sized from uneven-sized stands.

Metrics relating to understory development

The second and fourth significant pair of canonical variables again showed moderate correlations with two attributes of Lorenz curves, in this case with *BALM* ($r = -0.549$; $p = 0.000$) and *GC* ($r = -0.318$; $p = 0.055$; Table 2). Low values of *BALM* indicate a low proportion of large trees and a low *GC* value means size equality (Valbuena 2015). Both attributes show homogeneity in the stand population. In the set of sensor variables, moderate correlations were shown by *NDVI* metrics (Table 3). The negative correlation of *ndvi.Lkurt* ($r = -0.277$; $p = 0.098$) and positive of *ndvi.Min* ($r = 0.269$; $p = 0.107$) and *ndvi.Mean* ($r = 0.208$; $p = 0.216$) may be interpreted as presence of homogeneous vegetation, meaning the structural regularity of the vegetation cover. From the LiDAR metrics data set, *Height.KDEmodes* showed a positive relationship ($r = 0.333$; $p = 0.044$) and *Height. CRR* a negative one ($r = -0.292$; $p = 0.080$), as proxies for dense lower vegetation. All these variables together are related to even-sized structures. Hence, the fourth pair of canonical variables is a measure of size distribution, and therefore of the relative development of understory and overstory, and thus of the heterogeneity of the stand.

Conclusions

The most relevant result was to find that metrics derived from the multispectral sensor showed significant explanatory potential for the prediction of stand structural attributes. Although Valbuena et al. (2013) found no potential explanatory potential of the Difference Vegetation Index (Tucker 1979; a.k.a. redge index in Valbuena et al. 2013) median for the *GC*, here in the present work, we have demonstrated the possibilities of other spectral metrics derived from *NDVI* for the prediction of stand structural variables describing standing volume and heterogeneity (*GC, BALM*). In light of our new results, we concluded that metrics derived from the optical sensor have potential for complementing the information from the LiDAR sensor in describing structural properties of forest stands. We recommend the use of back-projecting for jointly exploiting the synergies of both sensors using similar types of metrics as they are customary in forestry applications of LiDAR.

The similarity in the interpretation of the first two pairs of canonical variables in this study, performed in a Scots pine stand in Spain, and that of Lefsky et al. (2005b) for different sites and species of North America, may be an indicator that LiDAR-derived height metrics can be used to predict structural forest variables of general stand development. These include height, volume, biomass, density, and cover, thus extending their utility to different forest types and different species. The LiDAR sensor has proven to be an excellent tool for the analysis of forest stand structure. On the other hand, complementary information from multispectral imagery has proven useful in the remaining canonical variable pairs to estimate the density and size heterogeneity of the stand. This adds further applications of the optical sensor to those reported earlier, such as those derived from incorporating canopy closure-related shadowing conditions at plot-

level or for detecting snags or vigor (Valbuena et al. 2013), or for extracting structural features directly from multispectral imagery (Gomez et al. 2011).

Acknowledgments

Disclosure statement

Funding

ORCID

Ruben Valbuena ⓘ http://orcid.org/0000-0003-0493-7581

References

Andersen, H. E., S. E. Reutebuch, and R. J. McGaughey. 2006. "A Rigorous Assessment of Tree Height Measurements Obtained Using Airborne Lidar and Conventional Field Methods." *Canadian Journal of Remote Sensing* 32 (5): 355–366. doi:10.5589/m06-030.

Arroyo, L. A., C. Pascual, and J. A. Manzanera. 2008. "Fire Models and Methods to Map Fuel Types: The Role of Remote Sensing." *Forest Ecology and Management* 256: 1239–1252.

Axelsson, P. 2000. "DEM Generation from Laser Scanner Data Using Adaptive TIN Models." *International Archives of Photogrammetry and Remote Sensing* 33 (Part B4 (110)): 110–117.

Bachofen, H., and A. Zingg. 2001. "Effectiveness of Structure Improvement Thinning on Stand Structure in Subalpine Norway Spruce (*Picea Abies* (L.) Karst.) Stands." *Forest Ecology and Management* 145: 137–149. doi:10.1016/S0378-1127(00)00581-8.

Baltsavias, E. P. 1999. "Airborne Laser Scanning: Basic Relations and Formulas." *ISPRS Journal of Photogrammetry and Remote Sensing* 542–3: 199–214. doi:10.1016/S0924-2716(99)00015-5.

Bright, B. C., J. A. Hicke, and A. T. Hudak. 2012. "Estimating Aboveground Carbon Stocks of a Forest Affected by Mountain Pine Beetle in Idaho Using Lidar and Multispectral Imagery." *Remote Sensing of Environment* 124: 270–281. doi:10.1016/j.rse.2012.05.016.

Buongiorno, J., S. Dahir, H. Lu, and C. Lin. 1994. "Tree Size Diversity and Economic Returns in Uneven-Aged Forest Stands." *Forest Science* 40: 83–103.

Chen, Y., and X. Zhu. 2013. "An Integrated GIS Tool for Automatic Forest Inventory Estimates of *Pinus Radiata* from Lidar Data." *GIScience & Remote Sensing* 50: 667–689.

Chu, H. J., C. K. Wang, S. J. Kong, and K. C. Chen. 2016. "Integration of Full-Waveform Lidar and Hyperspectral Data to Enhance Tea and Areca Classification." *GIScience & Remote Sensing*. doi:10.1080/15481603.2016.1177249.

Chuvieco, E. 2007. *Teledetección Ambiental*, 586. 3rd ed. Barcelona: Ariel Ciencia.

Cohen, W. B., T. K. Maiersperger, S. T. Gower, and D. P. Turner. 2003. "An Improved Strategy for Regression of Biophysical Variables and Landsat ETM+." *Remote Sensing of Environment* 84: 561–571.

Curtis, R. O., and D. D. Marshall. 2000. "Why Quadratic Mean Diameter?" *Western Journal of Applied Forestry* 153: 137–139.

Damgaard, C., and J. Weiner. 2000. "Describing Inequality in Plant Size or Fecundity." *Ecology* 81: 1139–1142.

Dörstel, C., K. Jacobsen, and D. Stallmann. 2003. "DMC-Photogrammeric Accuracy-Calibration Aspects and Generation of Synthetic DMC Images." *Optical 3-D Measurement Techniques* 6 (1): 74–82.

Estornell, J., B. Velázquez-Martí, I. López-Cortés, D. Salazar, and A. Fernández-Sarría. 2014. "Estimation of Wood Volume and Height of Olive Tree Plantations Using Airborne Discrete-Return Lidar Data." *GIScience & Remote Sensing* 51: 17–29.

Garcia, M., D. Riano, E. Chuvieco, J. Salas, and F. M. Danson. 2011. "Multispectral and Lidar Data Fusion for Fuel Type Mapping Using Support Vector Machine and Decision Rules." *Remote Sensing of Environment* 115 (6): 1369–1379.

Gomez, C., M. A. Wulder, F. Montes, and J. A. Delgado. 2011. "Forest Structural Diversity Characterization in Mediterranean Pines of Central Spain with Quickbird-2 Imagery and Canonical Correlation Analysis." *Canadian Journal of Remote Sensing* 37 (6): 628–642.

Gove, J. H. 2004. "Structural Stocking Guides: A New Look at an Old Friend." *Canadian Journal of Forest Research* 34 (5): 1044–1056.

Honkavaara, E., E. Ahokas, J. Hyyppä, J. Jaakkola, H. Kaartinen, R. Kuittinen, L. Markelin, and K. Nurminen. 2006. "Geometric Test Field Calibration of Digital Photogrammetric Sensors." *ISPRS Journal of Photogrammetry and Remote Sensing* 60: 387–399.

Hyyppä, J., H. Hyyppä, M. Inkinen, M. Engdahl, S. Linko, and Y. Zhu. 2000. "Accuracy Comparison of Various Remote Sensing Data Sources in the Retrieval of Forest Stand Attributes." *Forest Ecology and Management* 128: 109–120.

Knox, R. G., R. K. Peet, and N. L. Christensen. 1989. "Population Dynamics in Loblolly Pine Stands: Changes in Skewness and Size Inequality." *Ecology* 704: 1153–1167.

Koukoulas, S., and G. A. Blackburn. 2005. "Mapping Individual Tree Location, Height and Species in Broadleaved Deciduous Forest Using Airborne LIDAR and Multi-Spectral Remotely Sensed Data." *International Journal of Remote Sensing* 26: 431–455. doi:10.1080/0143116042000298289.

Lähde, E., O. Laiho, Y. Norokorpi, and T. Saksa. 1991. "The Structure of Advanced Virgin Forests in Finland." *Scandinavian Journal of Forest Research* 6: 527–537. doi:10.1080/02827589109382689.

Lefsky, M. A., W. B. Cohen, S. A. Acker, G. G. Parker, T. A. Spies, and D. Harding. 1999. "Lidar Remote Sensing of the Canopy Structure and Biophysical Properties of Douglas-Fir Western Hemlock Forests." *Remote Sensing of Environment* 70: 339–361. doi:10.1016/S0034-4257(99)00052-8.

Lefsky, M. A., A. T. Hudak, W. B. Cohen, and S. A. Acker. 2005a. "Geographic Variability in Lidar Predictions of Forest Stand Structure in the Pacific Northwest." *Remote Sensing of Environment* 95: 532–548. doi:10.1016/j.rse.2005.01.010.

Lefsky, M. A., A. T. Hudak, W. B. Cohen, and S. A. Acker. 2005b. "Patterns of Covariance between Forest Stand and Canopy Structure in the Pacific Northwest." *Remote Sensing of Environment* 95: 517–531. doi:10.1016/j.rse.2005.01.004.

Lei, X., W. Wang, and C. Peng. 2009. "Relationships between Stand Growth and Structural Diversity in Spruce-Dominated Forests in New Brunswick, Canada." *Canadian Journal of Forest Research* 39: 1835–1847. doi:10.1139/X09-089.

Lexerød, N. L., and T. Eid. 2006. "An Evaluation of Different Diameter Diversity Indices Based on Criteria Related to Forest Management Planning." *Forest Ecology and Management* 222: 17–28. doi:10.1016/j.foreco.2005.10.046.

Maltamo, M., J. Uuttera, and K. Kuusela. 1997. "Differences in Forest Stand Structure between Forest Ownership Groups in Central Finland." *Journal of Environmental Management* 51: 145–167. doi:10.1006/jema.1997.0140.

Mauro, F., R. Valbuena, J. A. Manzanera, and A. Garcia-Abril. 2011. "Influence of Global Navigation Satellite System Errors in Positioning Inventory Plots for Tree-Height Distribution Studies." *Canadian Journal of Forest Research* 411: 11–23. doi:10.1139/X10-164.

McArthur, R. H., and J. W. McArthur. 1961. "On Bird Species Diversity." *Ecology* 42: 594–598. doi:10.2307/1932254.

McElhinny, C., P. Gibbons, C. Brack, and J. Bauhus. 2005. "Forest and Woodland Stand Structural Complexity: Its Definition and Measurement." *Forest Ecology and Management* 218: 1–24. doi:10.1016/j.foreco.2005.08.034.

McGaughey, R. J. 2012. "FUSION/LDV: Software for LIDAR Data Analysis and Visualization." Version 3.10. Pacific Northwest Research Station. Seattle: USDA Forest Service.

Montgomery, R. A., and R. L. Chazdon. 2001. "Forest Structure, Canopy Architecture, and Light Transmittance in Tropical Wet Forests." *Ecology* 82: 2707–2718. doi:10.1890/0012-9658 (2001)082[2707:FSCAAL]2.0.CO;2.

Naesset, E. 2002. "Predicting Forest Stand Characteristics with Airborne Scanning Laser Using a Practical Two-Stage Procedure and Field Data." *Remote Sensing of Environment* 80: 88–99. doi:10.1016/S0034-4257(01)00290-5.

Ørka, H. O., T. Gobakken, E. Næsset, L. Ene, and V. Lien. 2012. "Simultaneously Acquired Airborne Laser Scanning and Multispectral Imagery for Individual Tree Species Identification." *Canadian Journal of Remote Sensing* 38: 125–138. doi:10.5589/m12-021.

Packalén, P., and M. Maltamo. 2006. "Predicting the Plot Volume by Tree Species Using Airborne Laser Scanning and Aerial Photographs." *Forest Science* 52: 611–622.

Packalén, P., A. Suvanto, and M. Maltamo. 2009. "A Two Stage Method to Estimate Species-Specific Growing Stock." *Photogrammetric Engineering & Remote Sensing* 75: 1451–1460. doi:10.14358/PERS.75.12.1451.

Pascual, C., A. García-Abril, W. B. Cohen, and S. Martín-Fernández. 2010. "Relationship between Lidar-Derived Forest Canopy Height and Landsat Images." *International Journal of Remote Sensing* 31 (5): 1261–1280. doi:10.1080/01431160903380656.

Pascual, C., A. Garcıa-Abril, L. G. Garcıa-Montero, S. Martın-Fernandez, and W. B. Cohen. 2008. "Object-Based Semi-Automatic Approach for Forest Structure Characterization Using Lidar Data in Heterogeneous *Pinus Sylvestris* Stands." *Forest Ecology and Management* 255: 3677–3685. doi:10.1016/j.foreco.2008.02.055.

Pohl, C., and J. L. Van Genderen. 1998. "Multisensor Image Fusion in Remote Sensing: Concepts, Methods and Applications." *International Journal of Remote Sensing* 19 (5): 823−854. doi:10.1080/014311698215748.

Reineke, L. H. 1933. "Perfecting a Stand-Density Index for even-aged forests." *Journal of Agricultural Research* 46: 627–638.

Rojo, A., and G. Montero. 1996. *El Pino Silvestre En La Sierra De Guadarrama*. Madrid: Ministerio de Agricultura Pesca y Alimentación. (in Spanish).

Rouse, J. W., R. H. Haas, J. A. Schell, D. W. Deering, and J. C. Harlan (1974). "*Monitoring the Vernal Advancement and Retrogradation (Greenwave Effect) of Natural Vegetation*." Type III Final Report, 371. Greenbelt: NASA Goddard Space Flight Center.

Saremi, H., L. Kumar, R. Turner, C. Stone, and G. Melville. 2014. "DBH and Height Show Significant Correlation with Incoming Solar Radiation: A Case Study of A Radiata Pine (*Pinus Radiata* D. Don) Plantation in New South Wales, Australia." *GIScience & Remote Sensing* 51: 427–444. doi:10.1080/15481603.2014.937901.

Sevilla, M. J. 1995. "A New Gravimetric Geoid in the Iberian Peninsula." *Bulletin d'Information* 77: 163–180.

Sherrill, K. R., M. A. Lefsky, and J. B. Bradford. 2008. "Forest Structure Estimation and Pattern Exploration from Discrete-Return Lidar in Subalpine Forests of the Central Rockies." *Canadian Journal of Forest Research* 38 (8): 2081–2096. doi:10.1139/X08-059.

St-Onge, A., and N. Achaichia. 2001. "Measuring Forest Canopy Height Using a Combination of LIDAR and Aerial Photography Data." *International Archives of Photogrammetry and Remote Sensing* 343 (W4): 131–137.

Torabzadeh, H., F. Morsdorf, and M. E. Schaepman. 2014. "Fusion of Imaging Spectroscopy and Airborne Laser Scanning Data for Characterization of Forest Ecosystems - A Review." *ISPRS Journal of Photogrammetry and Remote Sensing* 97: 25–35. doi:10.1016/j.isprsjprs.2014.08.001.

Tucker, C. 1979. "Red and Photographic Infrared Linear Combinations for Monitoring Vegetation." *Remote Sensing of Environment* 8: 127–150. doi:10.1016/0034-4257(79)90013-0.

Valbuena, R. 2014. "Integrating Airborne Laser Scanning with Data from Global Navigation Satellite Systems and Optical Sensors." In *Forestry Applications of Airborne Laser Scanning. Concepts and Case Studies*, edited by M. Maltamo, E. Næsset, and J. Vauhkonen, 63–88. Dordrecht: Springer. Managing Forest Ecosystems Series 27.

Valbuena, R. 2015. "Forest structure indicators based on tree size inequality and their relationships to airborne laser scanning." Dissertationes Forestales, 205. Finnish Society of Forest Sciences, Vantaa.

Valbuena, R., A. De Blas, S. Martín Fernández, M. Maltamo, G. J. Nabuurs, and J. A. Manzanera. 2013. "Within-Species Benefits of Back-Projecting Laser Scanner and Multispectral Sensors in Monospecific *Pinus Sylvestris* Forests." *European Journal of Remote Sensing* 46: 491–509. doi:10.5721/EuJRS20134629.

Valbuena, R., K. Eerikäinen, P. Packalen, and M. Maltamo. 2016. "Gini Coefficient Predictions from Airborne Lidar Remote Sensing Display the Effect of Management Intensity on Forest Structure." *Ecological Indicators* 60: 574–585. doi:10.1016/j.ecolind.2015.08.001.

Valbuena, R., F. Mauro, F. Arjonilla, and J. A. Manzanera. 2011. "Comparing Airborne Laser Scanning-Imagery Fusion Methods Based on Geometric Accuracy in Forested Areas." *Remote Sensing of Environment* 115: 1942–1954. doi:10.1016/j.rse.2011.03.017.

Valbuena, R., F. Mauro, R. Rodriguez-Solano, and J. A. Manzanera. 2010. "Accuracy and Precision of GPS Receivers under Forest Canopies in a Mountainous Environment." *Spanish Journal of Agricultural Research* 8: 1047–1057. doi:10.5424/sjar/2010084-1242.

Valbuena, R., F. Mauro, R. Rodriguez-Solano, and J. A. Manzanera. 2012b. "Partial Least Squares for Discriminating Variance Components in Global Navigation Satellite Systems Accuracy Obtained Under Scots Pine Canopies." *Forest Science* 582: 139–153. doi:10.5849/forsci.10-025.

Valbuena, R., P. Packalén, S. Martín-Fernández, and M. Maltamo. 2012a. "Diversity and Equitability Ordering Profiles Applied to the Study of Forest Structure." *Forest Ecology and Management* 276: 185–195. doi:10.1016/j.foreco.2012.03.036.

Valbuena, R., J. Vauhkonen, P. Packalén, J. Pitkanen, and M. Maltamo. 2014. "Comparison of Airborne Laser Scanning Methods for Estimating Forest Structure Indicators Based on Lorenz Curves." *ISPRS Journal of Photogrammetry and Remote Sensing* 95: 23–33. doi:10.1016/j.isprsjprs.2014.06.002.

Van Leeuwen, M., N. C. Coops, and M. A. Wulder. 2010. "Canopy Surface Reconstruction from a Lidar Point Cloud Using Hough Transform." *Remote Sensing Letters* 1 (3): 125–132. doi:10.1080/01431161003649339.

von Gadow, K., C. Zhang, C. Wehenkel, A. Pommerening, J. Corral-Rivas, M. Korol, S. Myklush, G. Hui, A. Kiviste, and X. Zhao. 2012. "Forest Structure and Diversity." In *Continuous Cover Forestry. Managing Forest Ecosystems 23*, edited by T. Pukkala and K. Von Gadow, 29–83. Dordrecht: Springer.

Wu, B., S. Tang, Q. Zhu, K. Y. Tong, H. Hu, and G. Li. 2015. "Geometric Integration of High-Resolution Satellite Imagery and Airborne Lidar Data for Improved Geopositioning Accuracy in Metropolitan Areas." *ISPRS Journal of Photogrammetry and Remote Sensing* 109: 139–151. doi:10.1016/j.isprsjprs.2015.09.006.

Zhang, C., Z. Xie, and D. Selch. 2013. "Fusing Lidar and Digital Aerial Photography for Object-Based Forest Mapping in the Florida Everglades." *GIScience & Remote Sensing* 50: 562–573.